Vacuum ultraviolet light production in capillar fibers

DESY Summer Student Program 2022

Giuseppe D'Ambruoso
Università degli Studi di Bari "Aldo Moro"

Supervisors:
Marc Seitz
Prof. Dr. Andrea Trabattoni

September 7, 2022

Contents

Abstract

The final aim of this project was the efficient production of vacuum ultraviolet light. Vacuum ultraviolet light is of great significance from both a theoretical and practical perspective since it can be used to gain a better understanding of nuclear properties and, therefore, give a strong impetus to the advancement in nuclear technologies. In fact, the energy gap between the ground state and the first excited level corresponds, for the nucleus of ^{229}Th, to the energy of a VUV photon $(\tilde{8}\,eV)$.
The goal of this project was pursued by mean of the realization of a device capable of creating VUV light starting from a NIR picosecond laser.

1 Theoretical background

The experimental setup developed in the project is based upon two nonlinear optical phenomena: second harmonic generation (SHG) and four-wave frequency mixing (FHG).

1.1 Wave equation in a homogeneus, nonmagnetic and nonlinear medium

Maxwell's equations in a homogeneous nonmagnetic and nonlinear medium in regions of space that contain no free charges or currents have the following form.

$$\nabla \cdot \tilde{\mathbf{E}}(\mathbf{r},t) = -\frac{1}{\varepsilon_0}\nabla \cdot \tilde{\mathbf{P}}(\mathbf{r},t)$$

$$\nabla \cdot \tilde{\mathbf{B}}(\mathbf{r},t) = 0$$

$$\nabla \times \tilde{\mathbf{E}}(\mathbf{r},t) = -\frac{\partial \tilde{\mathbf{B}}}{\partial t}(\mathbf{r},t)$$

$$\nabla \times \tilde{\mathbf{B}}(\mathbf{r},t) = -\frac{\varepsilon_0}{\mu_0}\frac{\partial \tilde{\mathbf{E}}}{\partial t}(\mathbf{r},t) + -\frac{1}{\mu_0}\frac{\partial \tilde{\mathbf{P}}}{\partial t}(\mathbf{r},t)$$

On the hypothesis that $\nabla(\nabla \cdot \tilde{\mathbf{E}}) \ll \nabla^2 \tilde{\mathbf{E}}$ (which is true in the cases of interest) and setting $\tilde{\mathbf{P}} := \tilde{\mathbf{P}}^{(1)} + \tilde{\mathbf{P}}^{(2)}$ and $\tilde{\mathbf{D}} := \tilde{\mathbf{D}}^{(1)} + \tilde{\mathbf{P}}^{(2)}$, it's easy to show that they are equivalent to the following equation.

$$\nabla^2 \tilde{\mathbf{E}}(\mathbf{r},t) - \frac{1}{\varepsilon_0 c^2}\frac{\partial^2 \tilde{\mathbf{D}}^{(1)}}{\partial t^2}(\mathbf{r},t) = \frac{1}{\varepsilon_0 c^2}\frac{\partial \tilde{\mathbf{P}}^{(2)}}{\partial t^2}(\mathbf{r},t) \tag{1}$$

If $\tilde{\mathbf{E}}(\mathbf{r},t) = \sum_n \tilde{\mathbf{E}}_n(\mathbf{r},t)$, then $\tilde{\mathbf{D}}(\mathbf{r},t) = \sum_n \tilde{\mathbf{D}}_n(\mathbf{r},t) = \sum_n \mathbf{D}_n(\mathbf{r})e^{i\omega_n t} + c.c.$ and Eq. 1 is valid for every component. Moreover, if dissipation can be neglected, then $\mathbf{D}_n^{(1)} = \varepsilon_0 \varepsilon_r(\omega_n) \cdot \mathbf{E}_n$ and:

$$\nabla^2 \tilde{\mathbf{E}}_n(\mathbf{r},t) - \frac{1}{\varepsilon_0 c^2}\frac{\partial^2 \tilde{\mathbf{E}}_n^{(1)}}{\partial t^2}(\mathbf{r},t) = \frac{1}{\varepsilon_0 c^2}\frac{\partial \tilde{\mathbf{P}}^{(2)}}{\partial t^2}(\mathbf{r},t) \qquad \forall n \tag{2}$$

Eq. 2 establishes the condition all the frequency components of the electric field and polarization density have to satisfy in every point of a homogeneous nonmagnetic and nonlinear medium which is devoid of free electric charges and currents. It also specifies that $P^{(2)}$ can lead to an electromagnetic wave only if its second derivative is not vanishing, that is, only if it corresponds to oscillating dipoles.

1.2 Second-order nonlinear susceptibility

Let us consider the circumstance in which the electric field incident upon a homogeneous nonmagnetic and nonlinear medium is the sum of distinct frequency components:

$$\tilde{\mathbf{E}}(\mathbf{r},t) = \sum_n \tilde{\mathbf{E}}_n(\mathbf{r},t) = \sum_n \mathbf{E}_n(\mathbf{r})e^{-i\omega_n t} + c.c. \equiv \sum_n \mathbf{E}(\omega_n)e^{-i\omega_n t} + c.c..$$

If $\tilde{\mathbf{P}} = \tilde{\mathbf{P}}^{(1)} + \tilde{\mathbf{P}}^{(2)}$ is the polarization density vector, then Eq. 2 establishes that $\tilde{\mathbf{P}}^{(2)}$ can be written as:

$$\tilde{\mathbf{P}}^{(2)}(\mathbf{r}, t) = \sum_n \mathbf{P}^{(2)}(\omega_n) e^{-i\omega_n t} + c.c.,$$

where the component $P^{(2)}(\omega_l)$ depends on the applied electric fields according to:

$$P_i^{(2)}(\omega_l) = \varepsilon_0 \sum_{j,k} \sum_{\omega_n + \omega_m = \omega_l} \chi_{ijk}^{(2)}(\omega_l, \omega_n, \omega_m) E_j(\omega_n) E_k(\omega_m). \quad (3)$$

The second-order tensor $\chi^{(2)}$ defined by Eq. 3 is known as *second-order susceptibility* and depends on the structural properties of the medium. It provides information about the reaction - in terms of polarization density - of the medium to a number of applied electric fields.

1.3 Second harmonic generation (SHG)

Let us consider the circumstance in which an electric field propagating along the z axis is applied to a second-order nonlinear optical medium:

$$\tilde{E}(z, t) = E(z) e^{-i\omega t} + c.c. = A e^{i(kz - \omega t)} + c.c.$$

Assuming that the polarization density induced by that electric field can be written in the form $\tilde{P} = \tilde{P}^{(1)} + \tilde{P}^{(2)}$ with $\tilde{P}^{(1)} = \varepsilon_0 \chi^{(1)} \tilde{E}$ and $\tilde{P}^{(2)} = \varepsilon_0 \chi^{(2)} \tilde{E}^2$, then:

$$\tilde{P}^{(2)}(z, t) = 2\varepsilon_0 \chi^{(2)} A^2 + (\varepsilon_0 \chi^{(2)} A^2 e^{-2i\omega t} + c.c.)$$

where $E(z) = A e^{ikz}$.
We see that the second-order polarization consists of the sum of two terms. According to Eq. 2, the first term does not lead to the generation of an electromagnetic wave since its second derivative is zero. On the contrary, the second term causes the generation of an electromagnetic wave with twice the frequency of the incident through a process known as *second harmonic generation.*
Eq. 2 holds for each frequency, in particular for 2ω. In this case, if the nonlinear surgent $\partial^2 P / \partial t^2$ is not too high, then

$$E'(z, t) \approx A'(z) e^{i(k'z - 2\omega t)} + c.c. \quad , \quad k' = \frac{2\omega n'}{c} \quad , \quad n'^2 = \varepsilon_r(2\omega)$$

can be considered a solution. Substituting it in Eq. 2 and assuming that $|d^2A/dz^2| << |k' dA/dz|$, we obtain a separable differential equation for $A'(z)$, which leads to:

$$A'(z) = \frac{4i\chi^{(2)} \omega^2 A}{k' c^2} e^{i\Delta k z} \quad , \quad \Delta k = 2k - k'.$$

This relationship can be used to easily calculate the average intensity over a period of the second harmonic wave as soon as it gets out from the crystal:

$$I'(L, \Delta k) = \frac{16\chi^{(2)} \omega^2 I^2}{\varepsilon_r(\omega) \sqrt{\varepsilon_r(2\omega)} \varepsilon_0 c^2} sinc^2 \left(\frac{L \Delta k}{2} \right) \quad (4)$$

where L is the length of the crystal and I is the average intensity over a period of the incident wave.

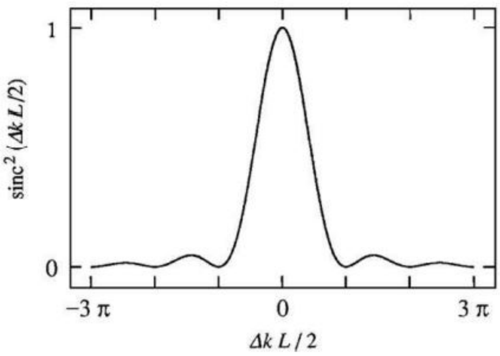

Figure 1: Intensity of the second harmonic wave.

As shown in Fig. 1, it reaches its maximum value when the following condition condition, known as *phase-matching condition*, is satisfied:

$$\Delta k = 0 \Leftrightarrow n(\omega) = n(2\omega). \tag{5}$$

This condition cannot be satisfied unless the refractive index depends on the direction of propagation of electromagnetic radiation, which is the case of negative uniaxial crystals. In them, refractive index obeys the equation:

$$\frac{1}{n_e(\theta)^2} = \frac{sin^2(\theta)}{\Psi_e^2} + \frac{cos^2(\theta)}{n_o^2} \tag{6}$$

where θ is the angle between the optic axis of the crystal and the propagation direction of the input beam, Ψ_e is the is the principal value of the extraordinary refractive index and n_o is the ordinary refractive index. Since Ψ_e is less than n_o for a negative uniaxial crystal, we choose the fundamental frequency to propagate as an ordinary wave and the second harmonic frequency to propagate as an extraordinary wave, in order that the birefringence of the material can compensate for the dispersion (see Fig. 2).

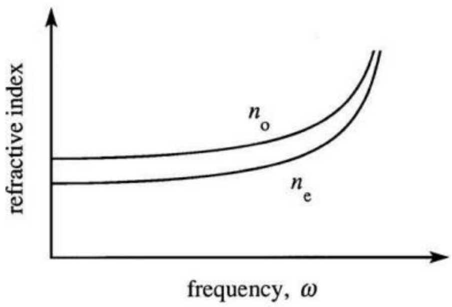

Figure 2: Dispersion of the refractive indices.

The phase-matching condition 5 then becomes (using Eq. 6):

$$\theta = \arcsin\sqrt{\left(\frac{\frac{1}{n_o(\omega)^2} - \frac{1}{n_o(2\omega)^2}}{\frac{1}{\Psi_e(2\omega)^2} - \frac{1}{n_o(2\omega)^2}}\right)}. \tag{7}$$

The previous relationship can be used to calculate the angle θ in order to maximize the second harmonic radiation's intensity.

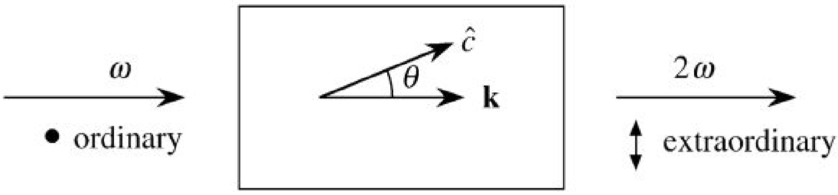

Figure 3: Geometry of angle-tuned phase matching of second-harmonic generation for the case of a negative uniaxial crystal.

1.4 Four-wave frequency mixing (FWM)

Let us next take into consideration the case in which the polarization density can be expressed as $\tilde{P} = \tilde{P}^{(1)} + \tilde{P}^{(2)} + \tilde{P}^{(3)}$, with $P^{(1)} = \varepsilon_0\chi^{(1)}\tilde{E}$, $P^{(2)} = \varepsilon_0\chi^{(2)}\tilde{E}^2$ and $P^{(3)} = \varepsilon_0\chi^{(3)}\tilde{E}^3$.

If $\tilde{E}(t) = E_1e^{-i\omega_1 t} + E_2e^{-i\omega_2 t} + c.c.$, then $P^{(3)}$ contains 16 different frequency components: $\omega_1, \omega_2, 2\omega_1 + \omega_2, 2\omega_1 - \omega_2, \omega_1 + 2\omega_2, \omega_1 - 2\omega_2, 3\omega_1$ and $3\omega_2$. The third-order nonlinear optical phenomena by which different frequency components are originated from two frequency components is called *four-wave frequency mixing.*

If the medium in which the frequency mixing occurs has an energy gap between the ground state and the first excited level of $2\hbar\omega_1$, then for resonance reasons the $(2\omega_1 - \omega_2)$ component prevails over the others. In such a case one speak of *resonance-enhanced four-wave frequency mixing.* An explanatory scheme of the process is shown in Fig. 4.

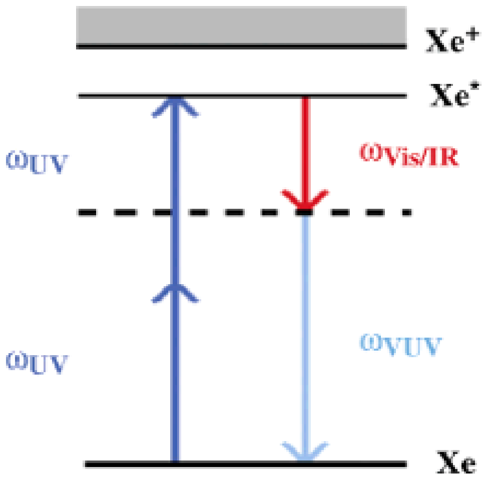

Figure 4: Resonance-enhanced FWM in Xenon gas.

2 Underlying idea of the project

The underlying idea of the project consists of dividing an initial NIR beam ($1020\,nm$) into two beams by mean of a beamsplitter.
One of the two beams go through two SHGs in cascade as to have an output wavelength of $255\,nm$. On the contrary, the other beam goes through such a sequence of reflective mirrors as to recombine with the first one with no optical path difference (which would decrease the FWM efficiency.
The two beams are recombined together with a beam recombiner and interact in a proper medium so to trigger the FWM.

3 Development of the project

The development of the project was divided into different phases.

3.1 First phase: designing of the setup

In the first phase, the experimental setup was designed. A schematic drawing of it is shown below.

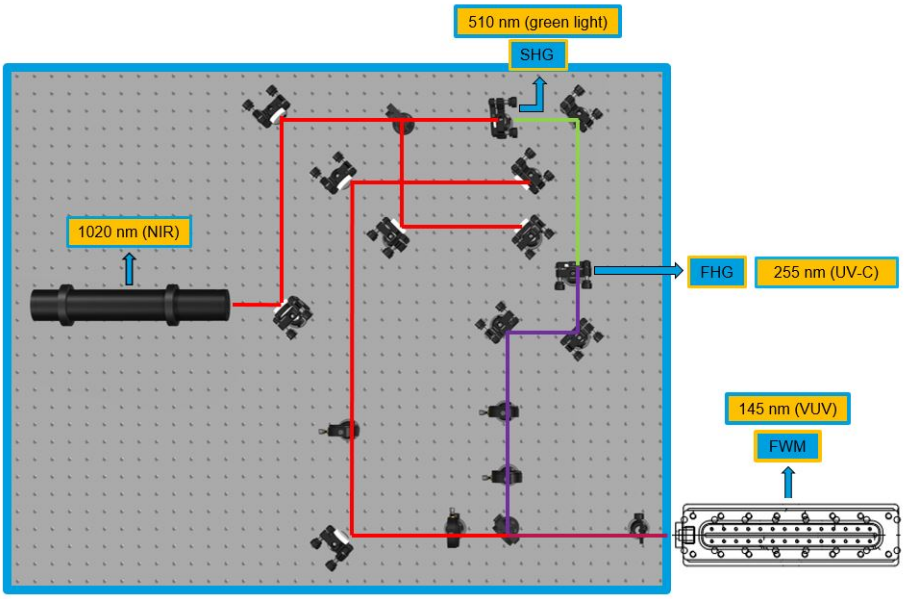

Figure 5: Drawing of the setup.

3.2 Second phase: implementation of the setup

3.2.1 Implementation of the second and fourth harmonic generation

For the two SHG in cascade two nonlinear crystals have been chosen: an LBO for the first SHG and a BBO for the second SHG (also known fourth harmonic generation, FHG). The choice fell on them because of their well-known efficient properties, in particular LBO was chosen for the SHG because of its high damage treshold.
The next step was to simulate their performance by mean of chi2D and chi3D in order to determine their optimal thickness and orientation with respect to the incident beam.
The simulation of the LBO was run as first. All the properties of the beam (shown in Tab. ??) were passed as input to chi2D and a 21-step sweep over different length of the crystal was carried out. The plots, shown in Fig. 7 and Fig. 6, suggest a thickness of $\tilde{0}.16\,mm$.

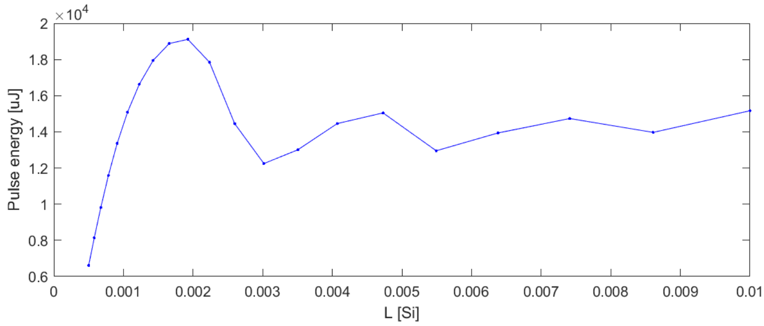

Figure 6: SH's energy as a function of the LBO's length.

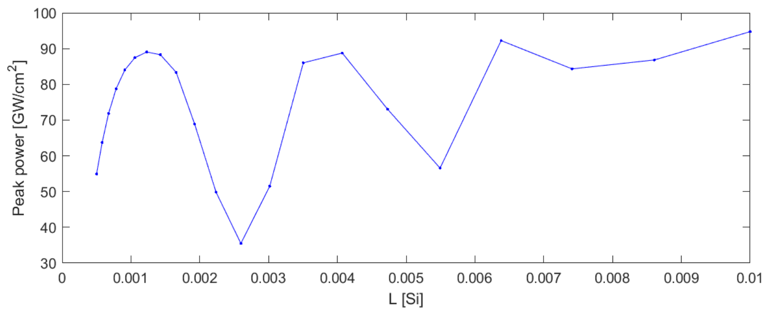

Figure 7: SH's peak intensity as a function of the LBO's length.

After that, a check for the absence of back-reflection rings in the intensity plot was performed with chi3D. The positive result is shown in Fig. 8.

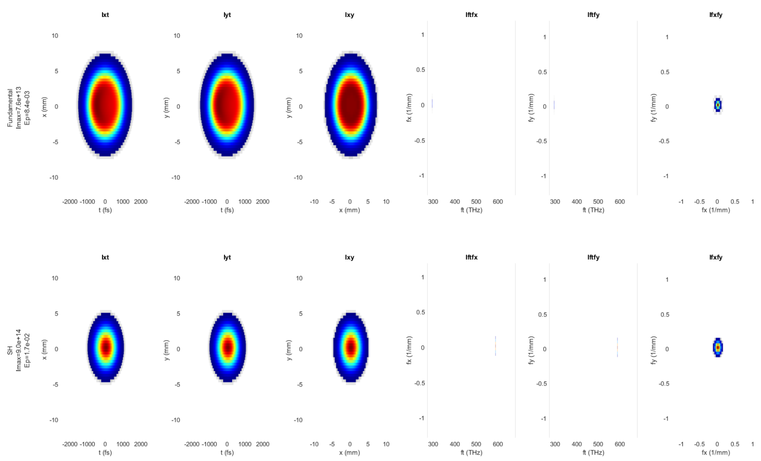

Figure 8: SH's beam profile.

For the simulation of the BBO, the output field of LBO was passed as input to chi3D and again a sweep over different lengths of the crystal was made. The results, confirmed by the absence of back-reflection rings, are shown in Fig. 9, Fig. 10 and Fig, 11.

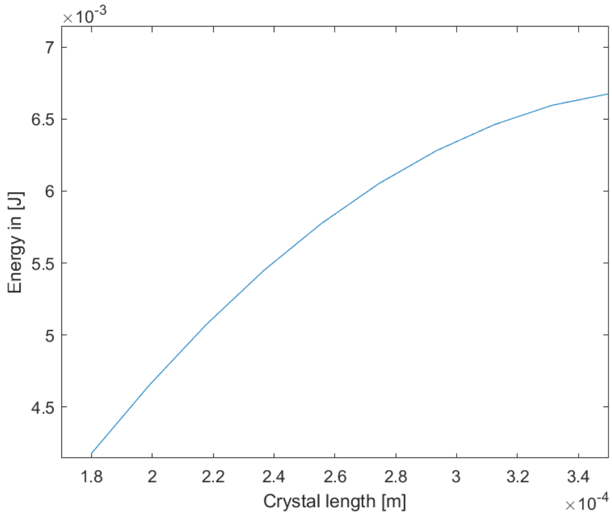

Figure 9: FH's energy as a function of the BBO's length.

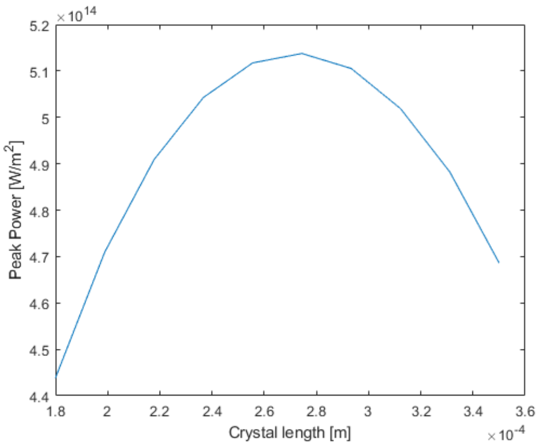

Figure 10: FH's peak intensity as a function of the BBO's length.

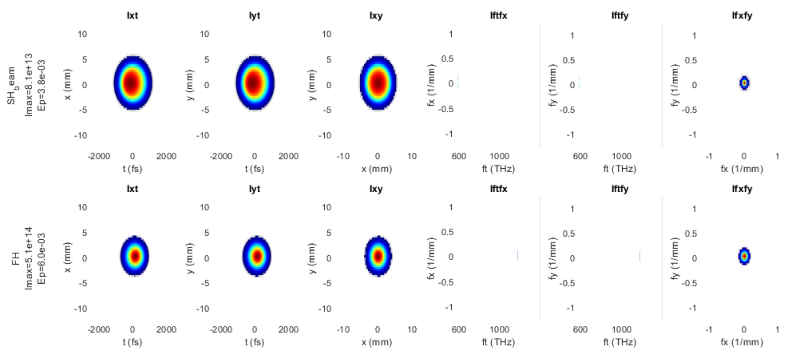

Figure 11: FH's beam profile.

Below is a table with the optimal lengths provided by the simulations and the corresponding values of energy peak, intensity peak and efficiency.

 10

$Crystal$	L $[mm]$	E_{in} $[mJ]$	E_{out} $[mj]$	I_{out}^{max} GW/cm^2	$Efficiency$ $\%$
BBO	1.26	25	16.7	89	66
LBO	0.27	16.7	11.6	78	69

Table 1

3.2.2 Implementation of the four-wave frequency mixing

As already explained in Par. 1.4, if the medium in which the frequency mixing occurs has an energy gap between the ground state and the first excited level of $2\hbar\omega_1$, then for resonance reasons the $(2\omega_1 - \omega_2)$ component prevails over the others. This means that, theoretically speaking, the best would be to use a gas with an energy gap equal to the energy of two UV-C photons. Unfortunately it can be shown that the experimental implementation of this idea is not satisfactorily efficient. Nevertheless, if the intensity of the input electric fields is high enough and it is kept high for a proper distance, a higher order phenomenon can be triggered: In fact, its energy gap is equivalent to the energy of two photons with wavelength $\lambda = 255\, nm$.
The FWM, being a nonlinear optical process, requires high intensity electric fields in order to be triggered. This is why the two input beams are focused onto the entrance of a thin hollow-core fiber (diamater = 50 nm). In fact, the small size of the focus spot (which has to be 65% the diamater of the fiber for coupling reasons) allows to reach high intensity, whereas the use of a thin fiber makes it possible to keep the intensity high thanks to total reflection.
In order to obtain the desired focusing of the two beams, each of them goes through a telescope made of two lenses positioned at a proper reciprocal distance. The choice of the lenses, as well as their positioning in the setup, will be carried out after my departure and it will be supported by software simulations.

3.3 Third phase: realization of the setup

The third phase consisted with the realization of the setup on a mobile breadboard. The positioning of the mirrors and lenses was performed by using a non dangerous green laser but then irises were added in order to make sure that the NIR laser hits all the optical devices in the right spot. The setup built is shown below.

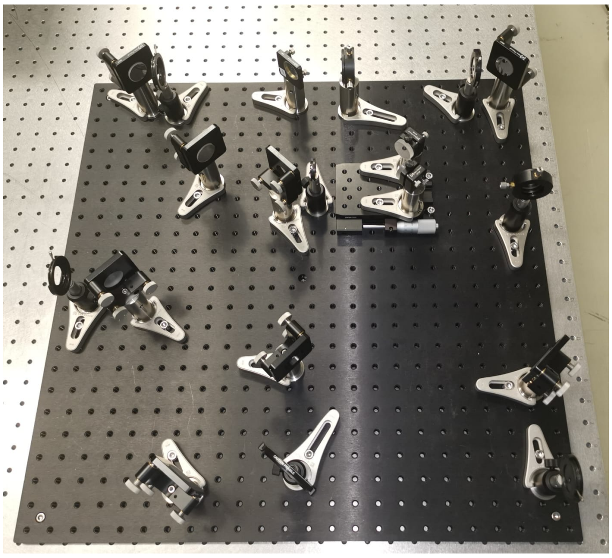

Figure 12: Experimental setup.

After my departure, the crystals will be inserted in the setup with such an inclination as to satisfy Eq. 7 and the lenses will be positioned at such a distance as to fulfill the focusing requirements explained in Par. 3.2.2.

References

[1] *chi23D*, http://www.chi23d.com/

[2] *High-power, 1-ps, all-Yb:YAG thin-disk regenerative amplifier*, https://opg.optica.org/ol/fulltext.cfm?uri=ol-41-6-1126&id=336917

[3] Robert W. Boyd, *Nonlinear optics* (1992)

[4] Fejer M., *Nonlinear optical frequency conversion*

[5] Belli F. et al., *Strong and weak seeded four-wave mixing in stretched gas-filled hollow capillary fibers*

[6] Belli F. et al., *Highly efficient deep UV generation by four-wave mixing in gas filled hollow-core photonic crystal fiber*

[7] Wittmann M. et al., *Generation of femtosecond VUV pulses and their application to time resolved spectroscopy in the gas phase*

[8] Hanna S.J. et al., *A new broadly tunable (7.4-10.2 eV) unable laser based VUV light source and its first application to aerosol mass spectrometry*